Applied Energy xxx (2014) xxx–xxx

Contents lists available at ScienceDirect

Applied Energy

journal homepage: www.elsevier.com/locate/apenergy

Temperature-dependent thermal properties of a paraffin phase change material embedded with herringbone style graphite nanofibers

Ronald J. Warzoha, Rebecca M. Weigand, Amy S. Fleischer *

Department of Mechanical Engineering, Villanova University, Villanova, PA 19085, United States

HIGHLIGHTS

- The thermal properties of a PCM with nanofibers are determined.
- The solid-phase thermal conductivity scales exponentially with volume fraction.
- The liquid-phase thermal conductivity is only enhanced beyond a critical percolation threshold.
- The nanoscale interface resistance depends on the nanoparticle's dimensionality.
- The thermal diffusivity and volumetric heat capacity of the nanoenhanced PCMs are found.

ARTICLE INFO

Article history:
Received 10 January 2014
Received in revised form 19 February 2014
Accepted 31 March 2014
Available online xxxx

Keywords:
Thermal conductivity
Thermal diffusivity
Herringbone graphite nanofiber
Phase change material
Thermal energy storage
Thermal boundary resistance

ABSTRACT

In many studies, carbon nanoparticles with high values of thermal conductivity (10–3000 W/m K) have been embedded into phase change thermal energy storage materials (PCMs) in order to enhance their bulk thermal properties. While a great deal of work to date has focused on determining the effect of these nanoparticles on a PCM's solid phase thermal properties, little is known about their effect on its liquid phase thermal properties. Thus, in this study, the effect of implanting randomly oriented herringbone style graphite nanofibers (HGNF, average diameter = 100 nm, average length = 20 μm) on the bulk thermal properties of an organic paraffin PCM (IGI 1230A, T_{melt} = 329.15 K) in both the solid and liquid phase is quantified. The bulk thermal conductivity, volumetric heat capacity and thermal diffusivity of HGNF/PCM nanocomposites are obtained as a function of temperature and HGNF volume loading level. It is found that the property enhancement varies significantly depending on the material phase. In order to explain the difference between solid and liquid phase thermal properties, heat flow at the nanoparticle–PCM and nanoparticle–nanoparticle interfaces is examined as a function of HGNF loading level and temperature. To do this, the solid and liquid phase thermal boundary resistances (TBRs) between the nanoparticles and the surrounding PCM and/or between contacting nanoparticles are found. Results suggest that the TBR at the HGNF–PCM interface is nearly double the TBR across the HGNF–HGNF interface in both solid and liquid phases. However, both the HGNF–PCM and HGNF–HGNF TBRs are at least an order of magnitude lower when the PCM is in its solid phase versus when the PCM is in its liquid phase. Finally, the effect of nanofiber concentration on the PCM's latent heat of fusion and melt temperature is investigated in order to determine the applicability of the HGNF/PCM nanocomposite in a wide variety of energy systems.

1. Introduction

The solid–liquid phase transition is of great interest to the scientific community for its association with thermal energy storage. A phase change material (PCM) stores thermal energy through the loosening or breaking apart of molecular or atomic bond structures when energy is transferred into the material. The stored heat can be discharged into a heat exchanger or the environment at a later time as the material recrystallizes. The amount of thermal energy that can be stored during this process is referred to as the latent heat of fusion and is an intrinsic material property. Organic PCMs (like paraffin) are known to possess a high value of latent heat of fusion (>200 kJ/kg) [1]. These materials are therefore considered to be excellent candidates for passively cooling electronics [2,3], storing solar-thermal energy [4–6] and for thermal comfort control

* Corresponding author. Tel.: +1 6105194996.
E-mail address: amy.fleischer@villanova.edu (A.S. Fleischer).

http://dx.doi.org/10.1016/j.apenergy.2014.03.091
0306-2619/

when incorporated into building materials [7,8]. More recently, PCMs have been used as the primary component in passive heat switch applications [9].

The use of organic PCMs for the aforementioned applications faces several major impediments, however. The greatest of these has been identified as their low thermal conductivities [10]. The thermal conductivity of most organic phase change materials is significantly less than 1 W/m K. When excessive heat loads are applied to these PCMs, the low thermal conductivity of the liquid causes it to superheat in close proximity to the heat source, while most of the PCM remains in its solid phase. As a result, only systems with short transient heat loads or those with a low applied heat flux are currently suitable for thermal management or thermal energy storage using organic paraffin PCMs [11,12]. In order to increase the utility of these PCMs, their thermal properties must be improved.

Enhancing the thermal conductivity of phase change materials can be accomplished in a variety of ways. In many early works, PCMs were simply embedded into heat sinks in order to increase the penetration of heat into the material [13–15]. However, the high density of the heat sink coupled with manufacturing limitations results in low compatibility with most state-of-the-art energy and electronics applications. Foams have also been identified as possible candidates for thermal conductivity enhancement of PCMs due to their high thermal conductivities (~180 W/m K for graphite [16]) and low densities [17–19]. One disadvantage of foams, however, is that they suppress natural convection during the phase transition. As a result, thermal charging rates (or melt times) are substantially increased within the PCM. Moreover, it is difficult to completely saturate most foams with an organic PCM without first displacing the air that is trapped between individual foam ligaments [19]. Finally, foam volumes also have manufacturing limitations and thus constrain applicability.

Recently, there has been strong interest in incorporating nanoparticles into organic phase change materials in order to enhance their thermal properties due to their high surface area-to-volume ratios and high thermal conductivities. Sanusi et al. [20] embedded three different types of graphite nanofibers (GNF) into a paraffin PCM (IGI 1230A, T_{melt} = 329.15 K) in order to analyze their effect on discharge times. The authors found that a 61% reduction in discharge time could be accomplished using a weight fraction of 10% Herringbone graphite nanofibers (HGNF). This reduction in discharge time makes the PCM a more attractive candidate for applications where heat is exchanged between materials, such as solar-thermal energy systems [21].

Several other works have found that nanoparticles enhance the thermal conductivity of PCMs, as reviewed by Fan and Khodadadi [10]. However, few of these studies describe the effect of nanoparticles on both the solid and liquid phase thermal properties of the PCM, which are equally important during melting and solidification processes. Even fewer studies report the thermal diffusivity in either material phase, making it difficult to determine the true enhancement of the PCM caused by the nanoparticles given the transient nature with which this material is used. Similarly, very little data exist concerning the nature of the physics that govern thermal transport between different types of nanoparticles and a surrounding organic PCM.

In this study, the nanoscale thermophysics governing the thermal conductivity enhancements of PCM nanocomposites are determined using a combination of experimental and analytical techniques. The primary focus of this work is to examine nanoscale interfacial thermophysics within the context of solid versus liquid bulk thermal properties. Here, the liquid thermal conductivity is a critically important parameter to consider during the PCM's solidification process. Consequently, in this paper we examine the heat flow physics at the nanoscale in order to help explain the differences in the thermal properties of the solid-phase PCM enhancements versus the liquid-phase PCM enhancements at different volume fractions. It is found that there are large discrepancies between heat flow across nanoparticle interfaces in the PCM solid and liquid phases, which result in extreme differences between the solid and liquid phase bulk thermophysical properties of the HGNF/PCM nanocomposites. These findings are related to the interfacial thermal resistance at the junction between other types of carbon-based nanoparticles and PCMs. Ultimately, the dimensionality of the nanoparticle is found to have a significant effect on thermal transport between the PCM and the nanoparticle(s) embedded within it. Additionally, the effect of the HGNF inclusions on the bulk latent heat of fusion and melt temperature is determined experimentally. The resulting insights allow for a better understanding of the mechanisms that govern heat flow within PCM nanocomposites and will allow for better design of these materials for state-of-the-art energy and electronics applications.

2. Analytical methods

The thermal characterization of nanostructures in nanofluids [22–24] and solid composites [25–27] has produced several valuable physical models that can be used to calculate their bulk thermal conductivities. These studies have also identified nanoscale phenomena that govern thermal transport within nanofluids and nanocomposites. Additional studies have experimentally determined the bulk thermal conductivity of paraffin PCMs with nanoinclusions [28–31]. Together, these studies [22–31] show varying degrees of influence of the nanoinclusions on bulk, room temperature thermal conductivity, and much attention has been placed on determining the physical mechanism(s) that govern these discrepancies.

Several physical models have been developed in order to determine the magnitude of the impact of nanoinclusions on the thermal conductivity of composite materials. The vast majority of these models are based on effective medium approximations. The simplest models assume that either: (1) all inclusions (nanoparticles) are connected and fully percolate throughout the medium or (2) all inclusions (nanoparticles) are separated and homogenously distributed within the medium. Models 1 and 2 are represented by the first two equations in Table 1.

In each equation in Table 1, k_c represents the effective thermal conductivity of the composite (W/m K), k_p is the nanoparticle thermal conductivity (W/m K), k_m is the thermal conductivity of the pure PCM (W/m K), φ_p is the volume fraction of nanoparticles within the PCM, φ_m is the volume fraction of PCM in the composite, a is the aspect ratio of the nanoparticle (ratio of length to diameter) and φ_{crit} is the percolation threshold for the HGNF. The models in the lower part of Table 1 (Eqs. (3), (4), (5) and (6)) were proposed by Nan et al. [33] (Eqs. (3) and (4)), Foygel et al. [34] (Eq. (5)) and Wemhoff [35] (Eq. (6)) and include the effect of nanoparticle orientation, the geometry of the nanoparticles and the nanoparticle–matrix and/or nanoparticle-nanoparticle thermal boundary resistance on the effective thermal conductivity of nanocomposite materials. In Eqs. (3) and (4), the parameters β, L and ε represent geometrical conditions of the nanoparticle inclusions (definitions of these parameters can be found in Nan et al. [33]). In Eq. (5), σ_0 is a preexponential factor that depends on the thermal conductivity and morphology of the nanoparticles and $t(a)$ is a conductivity exponent that is dependent on the aspect ratio of the nanoparticle. The criteria used for calculating both σ_0 and $t(a)$ can be found in Foygel et al. [34]. Finally, the parameters h_c, k_{pe} and ξ in Eq. (6) represent the nanoparticle–nanoparticle thermal contact resistance, the nanoparticle network effective thermal conductivity and a geometric constant that represents the nanoparticle network morphology, respectively. The function $g(k_{pe})$ is defined by Eq. (7).

Please cite this article in press as: Warzoha RJ et al. Temperature-dependent thermal properties of a paraffin phase change material embedded with herringbone style graphite nanofibers. Appl Energy (2014), http://dx.doi.org/10.1016/j.apenergy.2014.03.091

Table 1
Modified effective medium theory models for thermal conductivity of composites with nanostructures.

Name	Model	Equation Number	References
Parallel model (Upper bound)	$k_c = k_p \cdot \varphi_p + k_m \cdot \varphi_m$	1	Han and Fina [32]
Series model (Lower bound)	$k_c = \frac{1}{\frac{\varphi_m}{k_m} + \frac{\varphi_p}{k_p}}$	2	Han and Fina [32]
Spheres	$k_c = k_m \cdot \frac{k_p(1+2\beta) + 2k_m + 2\varphi_p(k_p(1-\beta) - k_m)}{k_p(1+2\beta) + 2k_m - \varphi_p(k_p(1-\beta) - k_m)}$	3	Nan et al. [33]
Completely disoriented ellipsoidal particles	$k_c = k_m \cdot \frac{3 + \varphi_p[2\varepsilon_{11}(1-L_{11}) + \varepsilon_{33}(1-L_{33})]}{3 - \varphi_p[2\varepsilon_{11}L_{11} + \varepsilon_{33}L_{33}]}$	4	Nan et al. [33]
Percolating ellipsoidal particles	$k_c = \sigma_0(\varphi_p - \varphi_{crit}(a))^{t(a)}$	5	Foygel et al. [34]
Percolating ellipsoidal particles	$k_e = \frac{\varphi_p^{1.5} \cdot g(k_{pe}) \cdot \xi(a) \cdot D}{2 \cdot \varphi_p \cdot (\frac{1}{k_c}) + \xi(a) \cdot D \cdot (\frac{1}{k_p})}$	6	Wemhoff [35]

$$g(k_{\mathrm{pe}}) = \left[\frac{1 - \frac{k_m}{k_{\mathrm{pe}}} \cdot (1-\alpha)}{1 - \frac{k_m}{k_c} \cdot (1-\alpha)}\right]^{3/2\cdot(1-\alpha)} \quad (7)$$

In the study presented here, the Nan et al. model [33] (Eq. (4)) is used to extrapolate the thermal boundary resistance (TBR) between a matrix material and an isolated nanoparticle, while the Foygel et al. model [34] (Eq. (5)) is used to determine the thermal boundary resistance at nanoparticle junctions. The Foygel et al. model [34] (Eq. (5)) is most often used in studies that calculate the TBR at nanoparticle–nanoparticle junctions and is therefore presently the standard physical model that is used as a basis for comparing the TBR at different nanoparticle–nanoparticle junctions between studies. While the model developed by Wemhoff [35] more accurately captures the nanoscale physics associated with heat flow at the nanoparticle–nanoparticle interface, it cannot be used here as the model assumes that there exists a uniform spatial and orientational distribution of straight nanoparticles within the host matrix. As is later shown in the SEM imaging analyses we performed, this assumption is violated and leads to a breakdown in the theory. Thus, only the models developed by Nan et al. [33] and Foygel et al. [34] are used to extract the thermal boundary resistance in this study.

The thermal boundary resistance across nanoparticle interfaces is a well-known phenomenon and can have a marked effect on the bulk thermal conductivity of a nanocomposite material [36,37]. However, the physical mechanisms that govern heat flow at these interfaces are still not well understood, though they have been attributed to discrepancies in the interface chemistry [38] and atomic ordering at nanoparticle interfaces [39,40]. Additional studies [41] have found that other nanoscale effects, such as Brownian motion, are negligible when compared to the thermal boundary resistance at nanoparticle interfaces, particularly in higher viscosity fluids. Therefore, in this study the TBR is considered to be the dominant mechanism that affects heat flow across nanoparticle interfaces.

3. Materials synthesis and characterization

The nanocomposite PCMs used in this study were prepared using a two-step method as described in Chintakrinda et al. [42]. The herringbone graphite nanofibers were prepared in house; the procedure for HGNF preparation is also described in Chintakrinda et al. [42]. In order to disperse the nanoparticles within the PCM, it was melted to a temperature of 353 K using a constant temperature hot plate. A sonicator was then used to disperse the nanoparticles within the PCM, which was set at 32 Hz and left to run for 2 h. The nanoenhanced PCM was then poured into a cylindrical copper vessel (see Fig. 1) and allowed to solidify. Nanocomposite PCMs with 0.05%, 0.1%, 0.2%, 0.3%, 0.4%, 2.8%, 5.8%, 8.5% and 11.4% volume fraction of HGNF were prepared.

The thermophysical properties of all of the pertinent materials used in this study are listed in Table 2. The nanofiber diameter and length listed in Table 2 were obtained in previous studies [43,44].

In order to solve for TBR, the physical properties for the materials of interest in this study (i.e. the values in Table 2) are substituted into the physical models (Eqs. (4) and (5)) in Table 1.

4. Experimental methods

Two separate experiments are used to obtain the thermophysical properties of the nanoenhanced PCMs. The first uses the transient plane source (TPS) technique to determine the thermal conductivity of the HGNF/PCM nanocomposites. In the second set of experiments, the volumetric heat capacity, latent heat of fusion and melt temperatures of the HGNF/PCM nanocomposite are determined using a Differential Scanning Calorimeter (DSC, TA Q200). Finally, density is measured using a simple volume displacement technique and is applied in the calculation of the temperature-dependent thermal diffusivity. Optical and SEM imaging studies are conducted in order to qualitatively determine when

Please cite this article in press as: Warzoha RJ et al. Temperature-dependent thermal properties of a paraffin phase change material embedded with herringbone style graphite nanofibers. Appl Energy (2014), http://dx.doi.org/10.1016/j.apenergy.2014.03.091

then nanoparticles begin to cluster and percolate. In this study, the percolation threshold determines which physical model is used to extract the nanoparticle interfacial thermal boundary resistance; when the nanoparticles are not percolating, the Nan model [33] is applied in order to calculate the nanoparticle–matrix TBR, whereas the model developed by Foygel et al. [34] is applied to PCMs with nanoparticles that form a network in order to calculate the nanoparticle–nanoparticle TBR. SEM images are produced using a Hitachi S-4800 Scanning Electron Microscope.

4.1. Thermal conductivity

The transient plane source technique is used to measure the thermal conductivity of the HGNF/PCM nanocomposites as a function of temperature. This technique uses a sensor that is immersed within a surrounding material. The sensor serves as both a heat source and a transient temperature measurement device; as the sensor heats up, so too does the surrounding semi-infinite material [47,48]. When the surrounding material has a low thermal diffusivity, the sensor temperature rise is large, whereas when the surrounding material has a high thermal diffusivity, the sensor temperature rise is small. Using the methods described in [47,48], the thermal conductivity and volumetric heat capacity of the surrounding material can be extracted simultaneously.

The TPS sensor shown in Fig. 1 is vertically immersed within the surrounding PCM. The PCM was contained within a cylindrical vessel and immersed in a constant temperature bath in order to maintain a constant internal temperature. The internal temperature of the PCM is monitored prior to testing using thermocouples in order to ensure that no thermal stratification occurred within the fluid.

In order to ensure that the experimental run times do not exceed the time to the onset of natural convection across the sensor face when the PCM is in its liquid form, the procedures developed in [47,48] are used. Because the specific heat capacity of each sample is known from the DSC measurements, the uncertainty of the TPS method is ±5.6% [47,48].

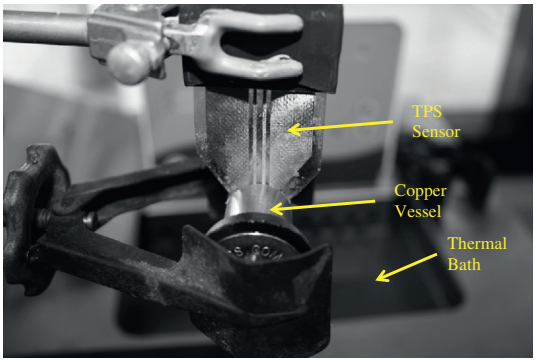

Fig. 1. TPS sensor immersed in copper vessel for the measurement of HGNF/PCM nanocomposite thermal conductivity as a function of temperature.

Table 2
Thermophysical properties of experimental materials.

Parameter	Value
PCM density (300 K)	880 kg/m^3
Nanofiber thermal conductivity	25 W/m K [45,46]
Nanofiber length	1–20 μm [43,44]
Nanofiber diameter	2–100 nm [43,44]
Nanofiber density	2.1 g/cm^3
PCM thermal conductivity	0.2 W/m K

4.2. Latent heat of fusion and melt temperature

The specific heat capacity, latent heat of fusion and melt temperature for each HGNF/PCM composite are calculated using DSC heating curves with a heating rate of 5 °C/min. The procedure for this experiment is described in ASTM Standard D4419 [49]. The melt temperature of the material is found by determining the minimum value of the endothermic peak within the heating curve. The latent heat of fusion value is determined by integrating over the endothermic peak(s). ASTM Standard E1269 [50] is used to determine the specific heat capacity of the liquid-phase HGNF/PCM nanocomposites as a function of temperature. The measurement uncertainties for these tests have been calculated previously [51] and are found to be ±1.9%. The density is obtained as a function of temperature by a volume displacement test; a 10 mL graduated cylinder with 0.1 mL intervals and 5 mL of water is placed on top of a constant temperature heater. Each sample's volume is measured via a conventional volume displacement technique, while its weight is measured using a Denver Instruments digital balance with an accuracy of ±0.0001 g. A measurement uncertainty of ±1.4% for this density experiment is calculated using the method described in [51]. A T-type thermocouple is used in order to ensure that there is minimal thermal stratification during testing ($\Delta T < 0.2$ K). The volumetric heat capacity for each HGNF/PCM nanocomposite is calculated as the product of density and specific heat capacity.

5. Results and discussion

5.1. Microscopy

Optical micrographs are produced in order to determine the HGNF distribution and cluster morphology within the PCM at low volume fractions. HGNF volume concentrations of 0.05%, 0.1%, 0.2%, 0.3% and 0.4% are synthesized and imaged in order to determine the critical volume fraction, ϕ_c (or the concentration of HGNF required to form a percolating network within the PCM) using a digital optical microscope (Olympus BX51 M). The HGNF distributions are imaged on glass slides that are dip coated in solutions with the aforementioned concentrations. Prior to dip coating, the glass slides are cleaned by sonication in a solution of NaOH for 20 min at a frequency of 10 Hz and then sonicated in deionized water for 10 min at 10 Hz. The micrographs are shown in Fig. 2.

The micrographs in Fig. 2 reveal the distribution of HGNF (dark regions) within the PCM (light regions) as a function of volume fraction. In Fig. 2(a), the HGNF particles are completely separated from one another, indicating that percolation does not exist at 0.05% volume fraction. As the volume fraction increases to 0.1% (Fig. 2(b)) and then 0.2% (Fig. 2(c)) the HGNFs begin to cluster, but do not form a completely percolating network. At a volume fraction of 0.3% (Fig. 2(d)), the HGNF are shown to fully percolate throughout the PCM, providing a thermally conductive network for heat flow. Beyond this point, the density of the HGNF network increases significantly (Fig. 2(e)).

Analytically, the percolation threshold for nanoparticle-based composites with nanoparticles whose aspect ratios are greater than 1 is represented by Eq. (8), which was derived by Foygel et al. [34] and later confirmed by Wemhoff [35].

$$\phi_c(a \gg 1) = \frac{0.6}{l \cdot d} \tag{8}$$

In Eq. (8), ϕ_c is the critical volume fraction at which percolating networks of nanofibers are formed, l is the length of the nanoparticle (m), d is the diameter of the nanoparticle (m) and a is the aspect ratio of the nanoparticle. Using the parameters in Table 2 and inserting them into Eq. (8), we calculate a percolation threshold, ϕ_c = 0.3 v%, which is supported by the images in Fig. 2.

Please cite this article in press as: Warzoha RJ et al. Temperature-dependent thermal properties of a paraffin phase change material embedded with herringbone style graphite nanofibers. Appl Energy (2014), http://dx.doi.org/10.1016/j.apenergy.2014.03.091

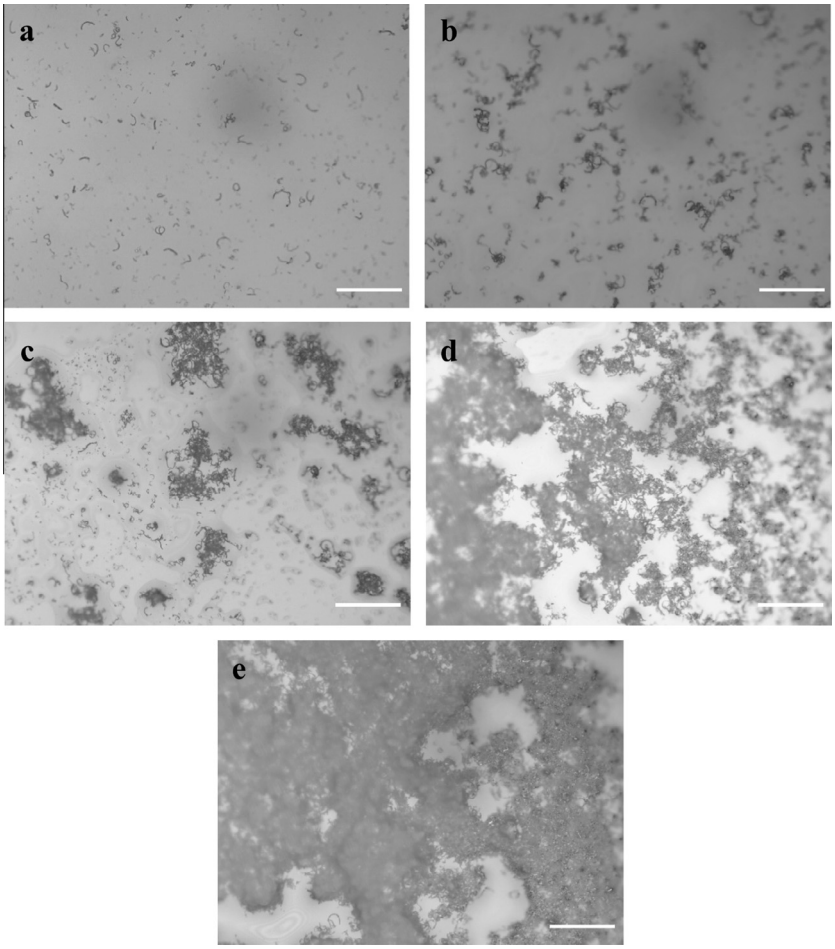

Fig. 2. Optical micrographs of HGNF distribution in PCM at volume concentrations of: 0.05%, (b) 0.1%, (c) 0.2%, (d) 0.3%, (e) 0.4%. Scale bars are shown in white and are 100 μm.

The images in Fig. 3 reveal the cluster morphology of HGNF beyond the percolation threshold. In these figures, the illuminated ellipsoids are the herringbone graphite nanofibers. For each volume fraction within the range of 2.8% to 11.4%, it is clear that the nanofibers percolate throughout the PCM. As the concentration of HGNF increases, the density of nanofibers per unit area also increases, yielding more pathways for thermal transport within the PCM. The morphology in Figs. 2 and 3 will be employed to support the physical models used to calculate the thermal boundary resistance at the HGNF–PCM and HGNF–HGNF interfaces. It should be noted that the nanofibers in Fig. 3 are coated with multiple layers of paraffin, and are found to have significantly smaller diameters when examined using a Transmission Electron Microscope, as detailed in previous work [43,44].

5.2. Thermal conductivity and nanoscale thermal boundary resistance

The thermal conductivity of the HGNF/PCM nanocomposites is determined as a function of temperature and volume loading level. Fig. 4(a) shows the thermal conductivity while Fig. 4(b) depicts the difference in thermal conductivity between the solid and liquid phases where the solid is measured at 293 K and the liquid is measured at 338 K.

Fig. 4 shows that the thermal conductivity of each HGNF/PCM composites is appreciably higher in the solid phase than in the liquid phase. Here, T_{melt} is the peak melt temperature of the base paraffin and is used to distinguish between the materials' solid phases and liquid phases. In the solid phase, there is a slight increase in the thermal conductivity with increasing temperature; however, the increase is within the reported uncertainty of the measurement technique. Thus, the thermal conductivity of the HGNF/PCM nanocomposite cannot be considered a strong function of temperature in the solid phase.

The variation between solid phase and liquid phase thermal properties is an important distinction for thermal energy storage and temperature control applications. In order to increase heat exchanger effectiveness in thermal energy storage systems, for instance, the PCM must be able to charge (heat up) and discharge (cool down) rapidly. During the PCM's charging state, an enhancement of the liquid-phase thermal conductivity is critically important when natural convection is suppressed due to the small pore sizes that are formed between contacting nanofibers. It should be noted that although the suppression of natural convection occurs when the PCM is saturated with nanofibers, the high surface area-to-volume ratios of the nanofibers allow a greater mass of PCM to be included in volume-constrained systems than within foams, primarily due to the manufacturing limitations of metallic and graphitic foams. In the discharge state, an enhancement in the liquid-phase thermal conductivity of the bulk PCM is necessary to achieve a rapid discharge of heat from the PCM and into the desired environment, irrespective of whether the nanoparticles percolate. This is primarily due to the fact that solidification is a diffusion-dominated process, where natural convection currents cease to exist. In both the charge and discharge states, an enhancement in the solid-phase thermal properties of the PCM is also critical to store and release heat rapidly. Thus, both solid phase

Please cite this article in press as: Warzoha RJ et al. Temperature-dependent thermal properties of a paraffin phase change material embedded with herringbone style graphite nanofibers. Appl Energy (2014), http://dx.doi.org/10.1016/j.apenergy.2014.03.091

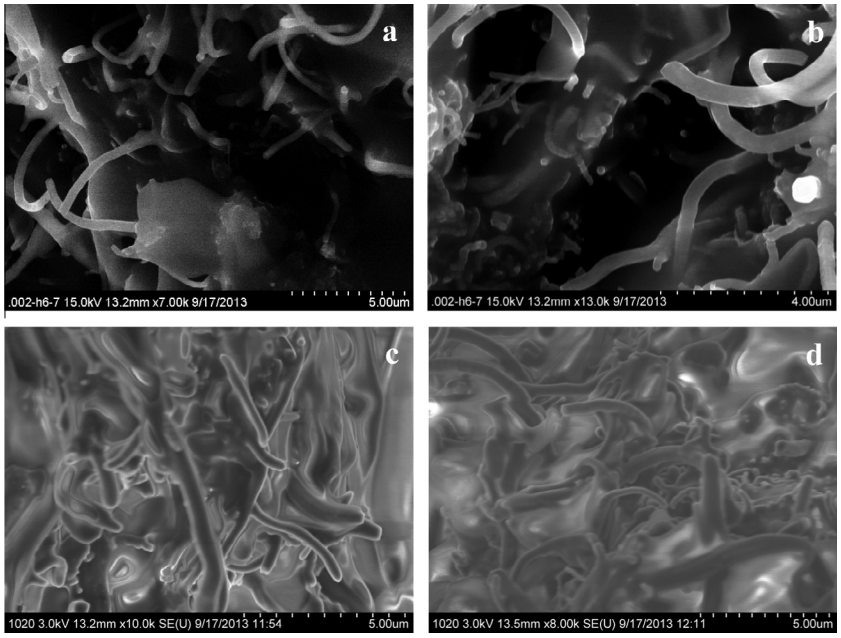

Fig. 3. SEM images of HGNF in PCM at: (a) 2.8 v%, (b) 5.8 v%, (c) 8.5 v%, (d) 11.4 v%.

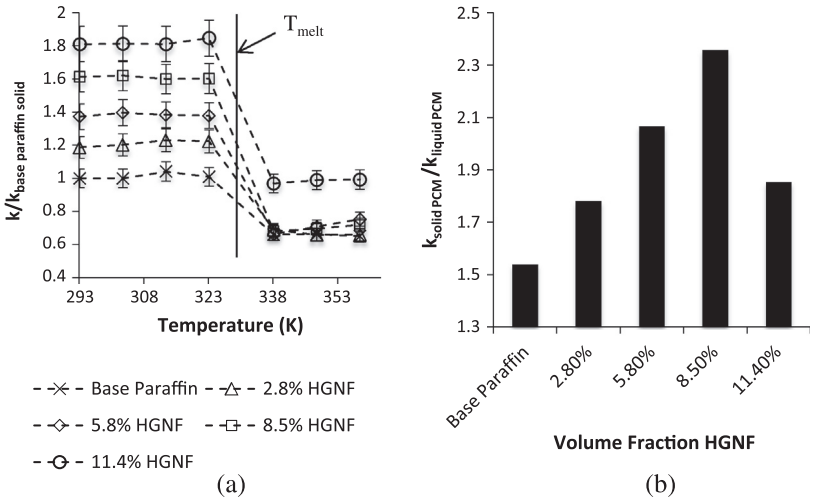

Fig. 4. (a) Temperature-dependent thermal conductivity of HGNF/PCM composites, (b) variance ratio (ratio of solid and liquid thermal conductivity).

and liquid phase thermal properties are of critical importance for sufficiently designing thermal energy storage systems. As is shown in Fig. 4(a), it is difficult to increase the thermal conductivity of the liquid phase PCM using highly conductive nanoparticles, even when fully percolating, as only the highest volume fraction (11.4%) shows any effect on the PCM's liquid phase thermal conductivity.

An analysis of the variance ratio (i.e. the ratio between solid and liquid phase thermal conductivity) of each HGNF/PCM composite confirms the difficulty associated with increasing the liquid phase thermal conductivity of organic PCMs (Fig. 4(b)). In this figure, it is clear that the variance ratio increases with increasing volume fraction, which means that the solid phase thermal conductivity increases at a higher rate than the liquid phase thermal conductivity as a function of HGNF volume loading level. This is an important result, as it indicates that a fully percolating network of nanoparticles does not promote heat flow in a liquid composite as well as it does in a solid composite. This trend continues until the volume fraction reaches 11.4% where the liquid phase thermal conductivity increases, reducing the variance ratio. This suggests that either: (1) there may be a secondary critical volume fraction of nanoparticles that will result in a decreased ratio between solid phase and liquid phase thermal conductivity or (2) the nanofiber networks are not stable enough to remain physically attached and a liquid layer forms between many of the junctions when the PCM is in its liquid phase, which is not overcome until a dense enough network is synthesized. These results are consistent with the results presented by Sanusi et al. [20], who report that when HGNF particles are above a critical threshold, the total PCM solidification time decreases by 50%.

In order to determine the physical mechanisms that control the differences between solid phase and liquid phase HGNF/PCM nanocomposite thermal conductivities, the TBR at the HGNF–PCM interface and the HGNF–HGNF interface is calculated by fitting the physical models developed by Nan et al. [33] and Foygel et al. [34] to the data in Fig. 5. Given that the thermal conductivity of

Please cite this article in press as: Warzoha RJ et al. Temperature-dependent thermal properties of a paraffin phase change material embedded with herringbone style graphite nanofibers. Appl Energy (2014), http://dx.doi.org/10.1016/j.apenergy.2014.03.091

each composite is not a strong function of temperature in either phase, each set of data points is averaged in order to extract the TBR at the nanoparticle–matrix interface (when the nanoparticles are not percolating) or the nanoparticle–nanoparticle interface (when the nanoparticles are percolating). The data are plotted as a function of volume fraction for each phase in Fig. 5(a and b). Additional data points are generated for solid and liquid phase thermal conductivities at volume concentrations below the percolation threshold (φ_p = 0.05%, 0.1%, 0.2%) in order to determine the TBR at the nanoparticle–PCM interface.

In order to fit the data to the Foygel model, σ_0 is used as a free parameter. In accordance with Ref. [34], $t(a)$ is determined as a function of the geometry of the HGNF clusters and was found to fit at $t(a) = 1.4$ based on two mathematical relations. Using these relations, the free parameter σ_0 is calculated to be $\sigma_0 = 20$ W/m K for solids and $\sigma_0 = 10$ W/m K for liquids. For the Nan model, the TBR is determined using Eq. (4) in accordance with the methods used by Wemhoff [35]. The Nan model is applied to the HGNF composite materials at volume fractions below the percolation threshold, φ_c. Thus, this range represents the magnitude of the TBR between an HGNF particle and the surrounding PCM. At HGNF volume fractions above φ_c, the Foygel et al. [34] model is applied using the relation described by Eq. (9) in order to determine the TBR at HGNF–HGNF interfaces.

$$R_{\mathrm{np-np}} = \left(\sigma_0 \cdot L \cdot \varphi_c^{t(a)}\right)^{-1} \tag{9}$$

Using the parameters listed in Table 2 and the regressions provided in Fig. 5, the TBR at HGNF interfaces in both the solid and liquid phases are calculated. In the solid phase, the TBR between the HGNF and the PCM is found to be $1.1 \cdot 10^{-4}$ m^2 K/W, which is nearly four orders of magnitude higher than the reported results for TBR at SWCNT- or MWCNT-matrix interfaces [52]. In SWCNT- or MWCNT-based composites, the TBR is between the outermost layer of carbon atoms and the host atoms, which tend to weakly bond to, and align at, the interface [39]. However, the HGNF used in this study are three-dimensional and non-uniform in nature, which may disrupt the arrangement of PCM molecules at the interface. Therefore, the TBR at nanoparticle interfaces may not depend on the size and type of the nanoparticle within the medium alone, but their dimensionality as well. When the HGNF are in contact with one another, the TBR was calculated to be $5.4 \cdot 10^{-5}$ m^2 K/W, which is significantly less than the TBR at the HGNF–PCM interface. Thus, it is also clear that heat flows preferentially along HGNF pathways rather than from HGNF to PCM, likely due to the acoustic phonon mismatch at the HGNF–PCM interface.

In the liquid phase, the TBR at the HGNF–PCM interface is found to be 1.8 10^{-4} m^2 K/W for volume concentrations of HGNF below the percolation threshold. This is higher than for the solid phase at the HGNF–PCM interface. The higher TBR in the liquid phase is likely caused by the freely moving PCM molecules at the HGNF–PCM junction, which form a much weaker bond with the HGNF carbon atoms than the van der Waals bonds formed at the alkane (PCM)-carbon (HGNF) interface. At the HGNF–HGNF interface within a liquid, the TBR is found to be $1.1 \cdot 10^{-4}$ m^2 K/W, which, surprisingly, is significantly higher than for the HGNF–HGNF interface in the solid phase. One possible explanation for this result is that a thin layer of liquid PCM develops between the nanoparticles upon thermal expansion. This possible liquid layer may be due to the thermal expansion of the PCM and may also be the cause of the increase in variance ratio as a function of HGNF loading level shown in Fig. 5(b) up to 8.5 v%. When the concentration is increased beyond this point, it is possible that enough of the fibers remain in contact with one another after thermal expansion that the heat can flow preferentially through the HGNF.

For comparison, the thermal conductivity data from Zheng et al. [9] is used to extract a TBR between two-dimensional graphite particles (>1 μm diameter) in both the solid and liquid phases of an organic PCM (hexadecane). Here, we fit $t(a)$ and σ_0 to the data provided by Zheng et al. [9] for both phases. For the solid phase, $t(a)$ is calculated to be 1.8 and σ_0 is found to equal 9000 W/m K. For the liquid phase, $t(a)$ is calculated to be 1.7, while σ_0 is calculated to be 4000 W/m K. The discrepancy in the calculated value for $t(a)$ is likely due to the difference in HGNF cluster morphology between the PCM's solid and liquid phases, which is confirmed by the optical micrographs supplied by Zhang et al. [9]. The resulting TBRs are calculated to be $2.2 \cdot 10^{-6}$ m^2 K/W and $2.4 \cdot 10^{-6}$ m^2 K/W when the graphite particles are percolating in solid and liquid phases, respectively. This is consistent with the results of this study; however the difference between TBR in the solid and liquid phases for the graphite particles in Zheng et al. [9] is lower than for the HGNF in this work. It is possible that the asymmetric, three-dimensional nature of the HGNF distorts the alignment of alkane atoms at the nanoparticle interface even more than the two-dimensional particles used by Zheng et al. Considering that the two-dimensional graphite nanoparticles result in a two-order of magnitude increase in TBR versus SWCNTs and MWCNTs [52] and the three-dimensional particles used in this study result in a four-order of magnitude increase in TBR versus SWCNTs and MWCNTs, it is highly likely that the dimensionality of the nanoparticle has an effect on the thermal performance of bulk nanocomposites. Regardless, it is clear that even for percolating networks of nanoparticles, the TBR across nanoparticle interfaces is higher in the liquid phase than in the solid phase. Thus, one challenge for thermal engineers moving forward is to fabricate a PCM nanocomposite with equivalently high thermal conductivity in both phases such that equivalently high rates of PCM charging and discharging can be achieved.

5.3. Volumetric heat capacity and thermal diffusivity

The temperature-dependent volumetric heat capacity and the thermal diffusivity of the HGNF/PCM nanocomposites are key parameters in the general form of the time-dependent energy equation that describes heat flow during sensible heating periods (i.e. before and after phase transitions). During a phase transition,

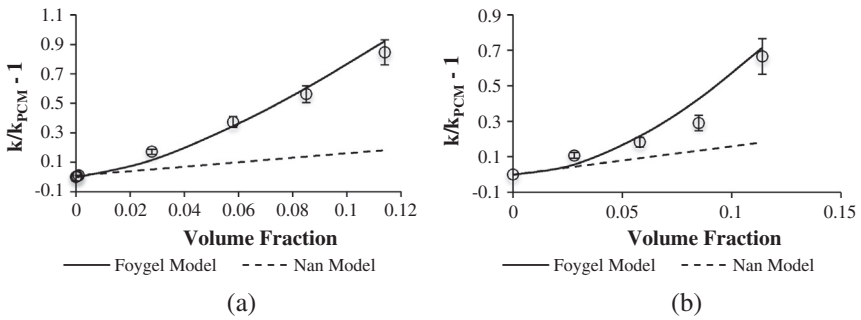

Fig. 5. Model fits for calculation of TBR in (a) solid and (b) liquid phases for HGNF/PCM composites.

Please cite this article in press as: Warzoha RJ et al. Temperature-dependent thermal properties of a paraffin phase change material embedded with herringbone style graphite nanofibers. Appl Energy (2014), http://dx.doi.org/10.1016/j.apenergy.2014.03.091

however, very little of the energy that is applied to the PCM results in its temperature increase. Instead, the energy is used to loosen or break apart the PCM's molecular or atomic bonds via latent heat. Thus, the PCM does not theoretically have a heat capacity during periods of phase transition due to the fact that energy is being absorbed into the PCM's bond structures. Eqs. (10) and (11) represent heat flow during periods of sensible and latent heating, respectively.

$$E = m \cdot c_p \cdot \Delta T \tag{10}$$

$$E = m \cdot L \tag{11}$$

In Eqs. (10) and (11), E represents heat flow (J), m represents the mass of the bulk material (kg), c_p is the specific heat capacity of the bulk material (J/kg K) and ΔT is the temperature increase from one state point to another (K). In Eq. (11), L is the value of the bulk material's latent heat during a phase transition. For the solid–liquid phase transition, this value represents latent heat of fusion (J/kg). In this study, an effective heat capacity is defined in Eq. (12) to determine an effective thermal diffusivity during periods of phase transition. This method has previously been used to determine time-dependent heat transfer rates into microencapsulated PCMs for microchannel cooling [53,54] and has been valuable in determining transient heat transfer coefficients for these systems. For this study, the effective heat capacity allows one to contrast the effective heat flow rates within the phase change material as a function of time.

$$c_p = L/\Delta T \tag{12}$$

The volumetric heat capacity is shown in Fig. 6 and the thermal diffusivity ($\alpha = k/\rho \cdot c_p$) in Fig. 7 for each of the HGNF/PCM nanocomposites as a function of temperature, phase and volume fraction.

In Fig. 6, the volumetric heat capacity is shown to decrease as a function of increasing HGNF volume fraction. In the solid phase, the effective volumetric heat capacity is calculated using Eq. (12) and is shown to decrease rapidly as a function of HGNF volume fraction. Subsequently, the effective volumetric heat capacity begins to taper off as the HGNF loading level is increased. The volumetric heat capacity during the solid–liquid phase transition is up to 2.8 times larger than for the solid phase HNGF/PCM nanocomposites and up to 4.4 times larger than for the liquid phase HGNF/PCM composites. As previously seen for the thermal conductivity of the HGNF/PCM nanocomposites (Fig. 5), it is difficult to alter the liquid phase volumetric heat capacity without achieving a critically dense network of nanoparticles.

The thermal diffusivity of each HGNF/PCM nanocomposite is shown as a function of temperature in Fig. 7. As a result of both the increase in the nanocomposites' solid phase thermal conductivities and the decrease in solid phase volumetric heat capacities, the thermal diffusivity increases linearly as a function of HGNF loading level from 293.15 K to 303.15 K. During the solid–liquid phase transition, the thermal diffusivity is significantly lower than either the solid or liquid phase thermal diffusivity, namely due to the energy conversion process during the phase change. Interestingly, as the HGNF loading level is increased, the difference between solid and liquid phase thermal diffusivity increases, in contrast to the difference between solid phase and liquid phase thermal conductivity. This phenomenon is not directly accounted for in some of the current computational simulations of solid–liquid phase change thermal energy storage systems [55], while others assume that the thermal conductivity of the PCM in its liquid phase scales linearly with increasing volume fraction of nanofibers [56], which is not shown to be the case in this study. It is therefore expected that these results will have important implications in the design and optimization of thermal energy storage systems in the future.

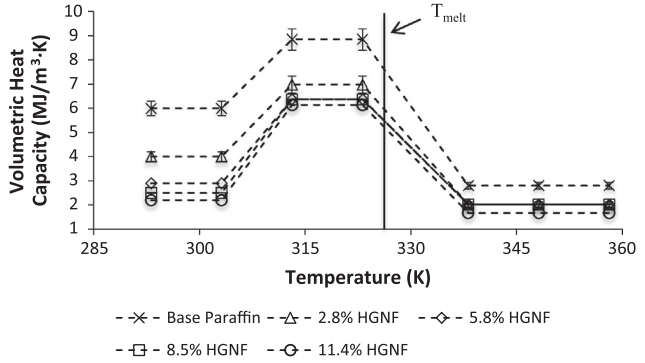

Fig. 6. Effective volumetric heat capacity of HGNF/PCM nanocomposites as a function of temperature.

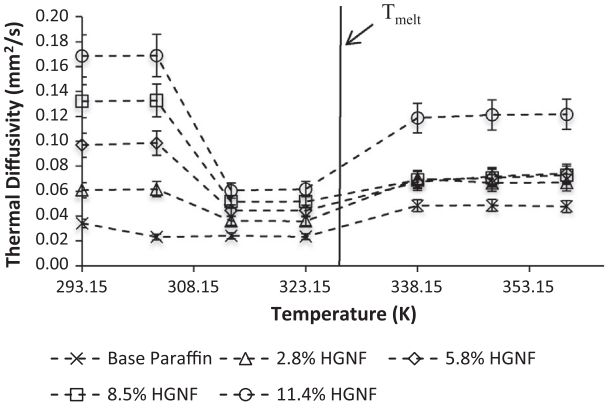

Fig. 7. Effective thermal diffusivity of HGNF/PCM nanocomposites as a function of temperature.

6. Latent heat of fusion and melt temperature

The melt temperature is defined as the minimum value of the DSC heating curves shown in Fig. 8, while the latent heat of fusion is obtained by integrating over the primary endothermic peak in each heating curve. The melt temperatures and latent heat of fusion values for pure paraffin and nanoenhanced paraffin are presented in Table 3.

In Fig. 8, two separate phase transitions occur. In the first, the PCM undergoes a solid–solid phase change, whereby its molecular structure is altered. In this case, thermal energy is stored due to a change in the molecular bonding structure of the alkane molecules. The presence of this solid–solid peak does contribute to the thermal energy storage of the PCM, but can potentially result in a delay in reaching the melt temperature. However, the influence of the

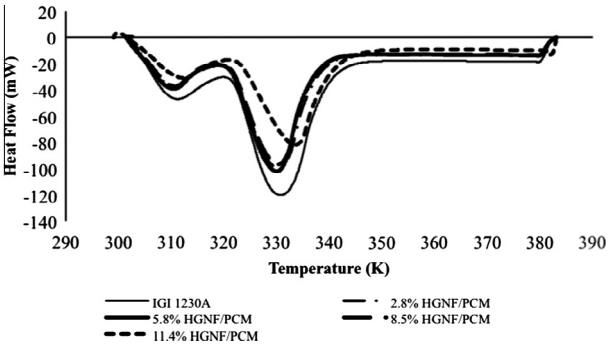

Fig. 8. DSC heating curves for HGNF/PCM nanocomposites.

Please cite this article in press as: Warzoha RJ et al. Temperature-dependent thermal properties of a paraffin phase change material embedded with herringbone style graphite nanofibers. Appl Energy (2014), http://dx.doi.org/10.1016/j.apenergy.2014.03.091

Table 3
Peak melt temperature and latent heat of fusion values for HGNF/PCM nanocomposites.

Sample	Peak melt temperature (K)	Latent heat of fusion (J/g)
IGI 1230A	327.75	271.6
2.8% HGNF	330.55	252.9
5.8% H-GNF	330.15	251.3
8.5% H-GNF	330.35	250.6
11.4% H-GNF	333.65	242.7

solid–solid phase change found to be minimal in this particular PCM; DSC results suggest that the solid–solid phase change contributes to less than 10% of the overall thermal energy storage density of the PCM, while a previous study conducted by the authors finds that the presence of this peak has a negligible effect on the total time it takes the PCM to reach its melt temperature [20].

As expected, the latent heat of fusion decreases with increasing volume fraction of HGNF; however, the PCM is able to retain ~90% of its latent heat value at all volume fractions included in this study, indicating that the nanofibers do not significantly reduce the PCM's ability to store thermal energy. Additionally, the melt temperature is altered by less than 1%. Thus, the addition of HGNF does not significantly impact the thermal energy storage characteristics of the organic PCM used in this study.

7. Conclusions

In this work, the thermal conductivity, volumetric heat capacity and thermal diffusivity were obtained for an organic phase change material (PCM) enhanced with different volume fractions of herringbone-style graphite nanofibers. Results show that the thermal conductivity of the HGNF/PCM nanocomposites increases exponentially in the PCM's solid phase as the nanoparticles begin to percolate. However, the PCM's liquid phase thermal conductivity does not increase significantly until the nanoparticles reach a critically dense state within the PCM, which is beyond the percolation threshold. The ratio of solid to liquid phase thermal conductivity (or variance ratio) was reported to support these findings; the variance ratio was shown to increase from 1.5 when the PCM was not saturated with nanoparticles to 2.4 at a volume fraction of 8.5% HGNF. The PCM's variance ratio did not decrease until a critically dense network of nanofibers existed in both its solid and liquid phases.

An analysis of the thermal boundary resistance at HGNF–PCM and HGNF–HGNF interfaces was completed to determine how well heat flows from the PCM to the nanoparticles and across the contact points along a three-dimensional network of nanostructures. It was shown that the thermal boundary resistance at the HGNF–PCM interface was much higher than the HGNF–HGNF interface in both the solid and the liquid phases, while the liquid phase HGNF–HGNF interfaces exhibited a thermal boundary resistance that was as much as an order of magnitude higher than the HGNF–HGNF thermal boundary resistance in the solid phase. These results were then compared to the interfacial thermal resistance at two-dimensional nanoparticle interfaces (graphene) and the results suggest that the thermal boundary resistance is substantially higher at the interface of a three-dimensional nanostructure than a two-dimensional nanostructure when the nanostructures are in contact with one another. Additionally, it was found that the solid and liquid phase thermal boundary resistances at nanoparticle junctions were nearly identical when the two-dimensional nanostructures were fully percolating.

The volumetric heat capacity, thermal diffusivity, latent heat of fusion and melt temperature were also obtained for the percolating HGNF/PCM nanocomposite materials. The results show that the volumetric heat capacity peaks during the period of solid–liquid phase transition, while it is lowest in the liquid phase. The disparity between solid and liquid phase thermal diffusivity was found to increase with increasing concentration of nanoparticles, in contrast to the results for thermal conductivity. It is therefore recommended that these physical phenomena be accounted for in computational and analytical studies in place of the general effective medium approximations that are used to predict these values. The latent heat of fusion for each nanocomposite was calculated to be within at least 90% of the base PCM value, while the melt temperature was altered by less than 1%. These results suggest that the presence of nanoparticles within the PCM does not significantly alter the PCM's performance in applications.

Acknowledgments

This material is based upon work supported by the National Science Foundation under Grant No. 0931507. Any opinions, findings, and conclusions or recommendations expressed in this material are those of the author(s) and do not necessarily reflect the views of the National Science Foundation. The research described in this paper has also been funded in part by the United States Environmental Protection Agency (EPA) under the Science to Achieve Results (STAR) Graduate Fellowship Program. EPA has not officially endorsed this publication and the views expressed herein may not reflect the views of the EPA.

References

[1] Rathod MK, Banerjee J. Thermal stability of phase change materials used in latent heat energy storage systems: a review. Renew Sustain Energy Rev 2013;18:246–58.
[2] Pal D, Joshi YK. Melting in a side heated tall enclosure by a uniformly dissipating heat source. Int J Heat Mass Transfer 2000;44:375–87.
[3] Chintakrinda K, Weinstein RD, Fleischer AS. A direct comparison of three different material enhancement methods on the transient thermal response of paraffin phase change material exposed to high heat fluxes. Int J Therm Sci 2011;50:1639–47.
[4] Mettawee E-BS, Assassa GMR. Thermal conductivity enhancement in a latent heat storage system. Sol Energy 2007;81:839–45.
[5] Nithyanandam K, Pitchumani R, Mathur A. Analysis of a latent thermocline storage system with encapsulated phase change materials for concentrating solar power. Appl Energy 2014;113:1446–60.
[6] Lecuona A, Nogueira J-I, Ventas R, Rodríguez-Hidalgo M-C, Legrand M. Solar cooker of the portable parabolic type incorporating heat storage based on PCM. Appl Energy 2013;111:1136–46.
[7] Charvát P, Klimeš L, Ostrý M. Numerical and experimental investigation of a PCM-based thermal storage unit for solar air systems. Energy Build 2014;68:488–97.
[8] Rouault F, Bruneau D, Sebastian P, Lopez J. Numerical modelling of tube bundle thermal energy storage for free-cooling of buildings. Appl Energy 2013;111:1099–106.
[9] Zheng R, Gao J, Wang J, Chen G. Reversible temperature regulation of electrical and thermal conductivity using liquid-solid phase transitions. Nat Commun 2011;2:289.
[10] Fan L, Khodadadi JM. Thermal conductivity enhancement of phase change materials for thermal energy storage: a review. Renew Sustain Energy Rev 2011;15:24–46.
[11] Alawadhi EM, Amon CH. PCM thermal control unit for portable electronic devices: experimental and numerical studies. IEEE Trans Components Package Technol 2003;26:116–25.
[12] Krishnan S, Murthy JY, Garimella SV. Analysis of solid-liquid phase change under pulsed heating. J Heat Transfer 2007;129:395.
[13] Yoo D-W, Joshi YK. Energy efficient thermal management of electronic components using solid-liquid phase change materials. IEEE Trans Device Mater Reliab 2004;4:641–9.
[14] Saha SK, Srinivasan K, Dutta P. Studies on optimum distribution of fins in heat sinks filled with phase change materials. J Heat Transfer 2008;130:034505.
[15] Nayak KC, Saha SK, Srinivasan K, Dutta P. A numerical model for heat sinks with phase change materials and thermal conductivity enhancers. Int J Heat Mass Transfer 2006;49:1833–44.
[16] Gallego NC, Klett JW. Carbon foams for thermal management. Carbon N Y 2003;41:1461–6.
[17] Lafdi K, Mesalhy O, Elgafy A. Merits of employing foam encapsulated phase change materials for pulsed power electronics cooling applications. J Electron Package 2008;130:021004.

Please cite this article in press as: Warzoha RJ et al. Temperature-dependent thermal properties of a paraffin phase change material embedded with herringbone style graphite nanofibers. Appl Energy (2014), http://dx.doi.org/10.1016/j.apenergy.2014.03.091

[18] Siahpush A, O'Brien J, Crepeau J. Phase change heat transfer enhancement using copper porous foam. J Heat Transfer 2008;130:082301.
[19] Warzoha R, Sanusi O, McManus B, Fleischer AS. Development of methods to fully saturate carbon foam with paraffin wax phase change material for energy storage. J Sol Energy Eng 2012;135:021006.
[20] Sanusi O, Warzoha R, Fleischer AS. Energy storage and solidification of paraffin phase change material embedded with graphite nanofibers. Int J Heat Mass Transfer 2011;54:4429–36.
[21] Salunkhe PB, Shembekar PS. A review on effect of phase change material encapsulation on the thermal performance of a system. Renew Sustain Energy Rev 2012;16:5603–16.
[22] Gao JW, Zheng RT, Ohtani H, Zhu DS, Chen G. Experimental investigation of heat conduction mechanisms in nanofluids. Clue on clustering. Nano Lett 2009;9:4128–32.
[23] Keblinski P, Phillpot S, Choi SU, Eastman J. Mechanisms of heat flow in suspensions of nano-sized particles (nanofluids). Int J Heat Mass Transfer 2002;45:855–63.
[24] Fan J, Wang L. Review of heat conduction in nanofluids. J Heat Transfer 2011;133:040801.
[25] Zhou T, Wang X, Mingyuan GU, Liu X. Study of the thermal conduction mechanism of nano-SiC/DGEBA/EMI-2,4 composites. Polymer (Guildf) 2008;49:4666–72.
[26] Pradhan NR, Duan H, Liang J, Iannacchione GS. The specific heat and effective thermal conductivity of composites containing single-wall and multi-wall carbon nanotubes. Nanotechnology 2009;20:245705.
[27] Chai Guangyu, Chen Quanfang. Characterization study of the thermal conductivity of carbon nanotube copper nanocomposites. J Compos Mater 2010;44:2863–73.
[28] Fukai J, Hamada Y, Morozumi Y, Miyatake O. Effect of carbon-fiber brushes on conductive heat transfer in phase change materials. Int J Heat Mass Transfer 2002;45:4781–92.
[29] Yavari F, Fard HR, Pashayi K, Rafiee MA, Zamiri A, Yu Z, et al. Enhanced thermal conductivity in a nanostructured phase change composite due to low concentration graphene additives. J Phys Chem C 2011;115:8753–8.
[30] Pincemin S, Py X, Olives R, Christ M, Oettinger O. Elaboration of conductive thermal storage composites made of phase change materials and graphite for solar plant. J Sol Energy Eng 2008;130:011005.
[31] Zeng JL, Cao Z, Yang DW, Sun LX, Zhang L. Thermal conductivity enhancement of Ag nanowires on an organic phase change material. J Therm Anal Calorim 2009;101:385–9.
[32] Han Z, Fina A. Thermal conductivity of carbon nanotubes and their polymer nanocomposites: a review. Prog Polym Sci 2011;36:914–44.
[33] Nan C-W, Birringer R, Clarke DR, Gleiter H. Effective thermal conductivity of particulate composites with interfacial thermal resistance. J Appl Phys 1997;81:6692.
[34] Foygel M, Morris R, Anez D, French S, Sobolev V. Theoretical and computational studies of carbon nanotube composites and suspensions: electrical and thermal conductivity. Phys Rev B 2005;71:104201.
[35] Wemhoff AP. Thermal conductivity predictions of composites containing percolated networks of uniform cylindrical inclusions. Int J Heat Mass Transfer 2013;62:255–62.
[36] Yang J, Yang Y, Waltermire SW, Wu X, Zhang H, Gutu T, et al. Enhanced and switchable nanoscale thermal conduction due to van der Waals interfaces. Nat Nanotechnol 2011;7:91–5.
[37] Prasher R. Acoustic mismatch model for thermal contact resistance of van der Waals contacts. Appl Phys Lett 2009;94:041905.
[38] Xu Z, Buehler MJ. Nanoengineering heat transfer performance at carbon nanotube interfaces. ACS Nano 2009;3:2767–75.
[39] Babaei H, Keblinski P, Khodadadi JM. Thermal conductivity enhancement of paraffins by increasing the alignment of molecules through adding CNT/graphene. Int J Heat Mass Transfer 2013;58:209–16.
[40] Babaei H, Keblinski P, Khodadadi JM. Improvement in thermal conductivity of paraffin by adding high aspect-ratio carbon-based nano-fillers. Phys Lett A 2013;377:1358–61.
[41] Babaei H, Keblinski P, Khodadadi JM. A proof for insignificant effect of Brownian motion-induced micro-convection on thermal conductivity of nanofluids by utilizing molecular dynamics simulations. J Appl Phys 2013;113:084302.
[42] Chintakrinda K, Warzoha RJ, Weinstein RD, Fleischer AS. Quantification of the impact of embedded graphite nanofibers on the transient thermal response of paraffin phase change material exposed to high heat fluxes. J Heat Transfer 2012;134:071901.
[43] Bessel CA, Laubernds K, Rodriguez NM, Baker RTK. Graphite nanofibers as an electrode for fuel cell applications. J Phys Chem B 2001;105:1115–8.
[44] Rodriguez NM. A review of catalytically grown carbon nanofibers. J Mater Res 2011;8:3233–50.
[45] Yu C, Saha S, Zhou J, Shi L, Cassell AM, Cruden BA, et al. Thermal contact resistance and thermal conductivity of a carbon nanofiber. J Heat Transfer 2006;128:234.
[46] Khadem MH, Wemhoff AP. Thermal conductivity predictions of herringbone graphite nanofibers using molecular dynamics simulations. J Chem Phys 2013;138:084708.
[47] Warzoha RJ, Fleischer AS. Determining the thermal conductivity of liquids using the transient hot disk method. Part I: Establishing transient thermal-fluid constraints. Int J Heat Mass Transf 2014;71:779–89.
[48] Warzoha RJ, Fleischer AS. Determining the thermal conductivity of liquids using the transient hot disk method. Part II: Establishing an accurate and repeatable experimental methodology. Int J Heat Mass Transfer 2014;71:790–807.
[49] ASTM D4419-90(2010) Standard Test Method for Measurement of Transition Temperatures of Petroleum Waxes by Differential Scanning Calorimetry (DSC). West Conshohocken, PA: 2010.
[50] ASTM E1269-11 Standard Test Method for Determining Specific Heat Capacity by Differential Scanning Calorimetry. West Conshohocken, PA: 2011.
[51] Warzoha RJ, Weigand R, Rao A, Fleischer AS. Experimental characterization of the thermal diffusivity of paraffin phase change material embedded with herringbone style graphite nanofibers. ASME Summer Heat Transf. Conf., Rio Grande, PR: 2012. p. 307–15.
[52] Buongiorno J, Venerus DC, Prabhat N, Mckrell T, Townsend J, Christianson R, et al. A benchmark study on the thermal conductivity of nanofluids. J Appl Phys 2009;106:094312.
[53] Sabbah R, Farid MM, Al-Hallaj S. Micro-channel heat sink with slurry of water with micro-encapsulated phase change material: 3D-numerical study. Appl Therm Eng 2009;29:445–54.
[54] Kuravi S, Kota KM, Du J, Chow LC. Numerical investigation of flow and heat transfer performance of nano-encapsulated phase change material slurry in microchannels. J Heat Transfer 2009;131:062901.
[55] Seyf HR, Zhou Z, Ma HB, Zhang Y. Three dimensional numerical study of heat-transfer enhancement by nano-encapsulated phase change material slurry in microtube heat sinks with tangential impingement. Int J Heat Mass Transfer 2013;56:561–73.
[56] Dhaidan NS, Khodadadi JM, Al-Hattab TA, Al-Mashat SM. Experimental and numerical investigation of melting of NePCM inside an annular container under a constant heat flux including the effect of eccentricity. Int J Heat Mass Transfer 2013;67:455–68.

Please cite this article in press as: Warzoha RJ et al. Temperature-dependent thermal properties of a paraffin phase change material embedded with herringbone style graphite nanofibers. Appl Energy (2014), http://dx.doi.org/10.1016/j.apenergy.2014.03.091